

Improving the diurnal cycle of convection in GCMs

R. A. Stratton* and A. J. Stirling

Met Office, Exeter, UK

*Correspondence to: R. A. Stratton, Met Office, FitzRoy Road, Exeter EX1 3PB, UK.

E-mail: rachel.stratton@metoffice.gov.uk

The Met Office single-column model is used to examine the development phase of the diurnal cycle of tropical convection over land by comparing against previous results from an idealized cloud-resolving model study. Changing the deep convective parametrization over land to make the entrainment vary with the height of the lifting condensation level reduces the depth of the convection early in the day. The changes made to improve the early phase of diurnal cycle over land are tested in an atmosphere-only version of the Met Office Hadley Centre climate model and result in an improvement in the amplitude and timing of the diurnal peak in precipitation over land. Copyright © 2011 British Crown copyright, the Met Office. Published by John Wiley & Sons Ltd.

Key Words: convection; diurnal cycle; entrainment

Received 2 March 2011; Revised 24 October 2011; Accepted 13 November 2011; Published online in Wiley Online Library 15 December 2011

Citation: Stratton RA, Stirling AJ. 2012. Improving the diurnal cycle of convection in GCMs. *Q. J. R. Meteorol. Soc.* **138**: 1121–1134. DOI:10.1002/qj.991

1. Introduction

Convection, particularly over tropical land, has a strong diurnal cycle. Most climate and global numerical weather prediction (NWP) models fail to correctly simulate the observed convective diurnal cycle (Yang and Smith, 2006), tending to develop deep convection too early in the day (e.g. Yang and Slingo, 2001; Guichard *et al.*, 2004; Grabowski *et al.*, 2006). In the Met Office Unified Model (Cullen, 1993), deep tropical convection over land is typically initiated within one or two time steps of sunrise, and quickly reaches the upper troposphere, yet in reality convection grows more gradually from shallow to deep. This study sets out to improve the representation of the diurnal cycle using adaptations to the Gregory and Rowntree (1990) mass flux scheme.

The cloud-resolving model (CRM) study of Guichard *et al.* (2004) shows, that provided CRMs have high enough resolution, i.e. 1 km or less, they are capable of correctly modelling the timing of the diurnal cycle of convection over the Atmospheric Radiation Measurement (ARM) Great Plains site. A number of recent CRM studies have looked at the development phase of the diurnal cycle over land. Grabowski *et al.* (2006) look at a case based on observations from the Large-scale Biosphere–Atmosphere (LBA) experiment in Amazonia from 23 February 1999. They find

that a number of CRMs are able to correctly simulate the growth of shallow convection and its transition to deep convection. Grabowski *et al.* (2006) suggest that as the cloud widths increase with time then the entrainment rate may vary accordingly. This is also confirmed by Khairoutdinov and Randall (2006), who find that deep convection tends to occur once the clouds have reached a certain horizontal size, and they suggest that this size is controlled by the scale of the inhomogeneity in the boundary layer moist static energy field introduced by cold pools. Del Genio and Wu (2010), using a CRM for the Tropical Warm Pool-International Cloud Experiment (TWP-ICE) to study the transition from shallow to deep convection over land, find that the entrainment rate weakens as the convection over land deepens. A CRM study by Kuang and Bretherton (2006) looking at the transition of shallow to deep convection over the sea again concludes that as the convection generates cold pools, this leads to larger cloud bases and smaller entrainment rates.

A recent observational study of data from the ARM Great Plains site Zhang and Klein (2010) finds that relative humidity and stability in the region of 2–4 km is important in determining when in the day and whether convection transitions from shallow to deep on days when the forcing is purely diurnal. They also find that boundary layer inhomogeneity is higher on days when deep

diurnal convection occurs, the inhomogeneity being further increased after precipitation starts.

We draw on results from an idealized CRM study described in Stirling and Stratton (2011), using a variety of relative humidities and stabilities, which showed that the entrainment rates during the development phase are significantly higher than those used in the Gregory–Rowntree mass flux scheme, and that the buoyancy in the cloud core controls the depth of convection. This buoyancy is controlled by the amount of environmental air reaching the cloud core, and this amount decreases as the horizontal size of the clouds increases with time.

A study of diurnal convection in the ECMWF model Bechtold *et al.* (2004) found that the timing could be improved by increasing the entrainment rates and altering the convective triggering. A recent study using a regional model over the maritime continent by Wang *et al.* (2007) looking at the impact of altering the entrainment/detrainment rates in a Tiedtke mass flux scheme (Tiedtke, 1989) finds that increasing the entrainment/detrainment rates for both deep and shallow convection delays the diurnal cycle of convection.

Rio *et al.* (2009) take a different approach to improving the diurnal cycle of convection over land. They modify the triggering and closure of their deep convection scheme (Emanuel, 1991) to link it to the sub-cloud processes. Deep convection is initiated if the kinetic energy of the thermals exceeds the convective inhibition (CIN) similarly to Kuang and Bretherton (2006). This then delays the start of deep convection as it takes time for the thermals to build up enough energy to overcome the CIN. The deep closure is related to the energy of the thermals and to the kinetic energy in cold-pool wakes in the boundary layer generated by convective downdraughts. While this approach looks promising, it relies on the accurate representation of CIN, and therefore depends on adequate resolution of the top of the boundary layer, which at current Global Circulation Model (GCM) resolutions may be insufficient.

In this study we use preliminary findings on the entrainment rates from Stirling and Stratton (2011) as a basis for changing the Unified Model (UM) convection parametrization over land. We test these modifications in a series of single-column model (SCM) experiments that are designed to match the CRM experiments performed in Stirling and Stratton (2011), and then apply these changes in a full GCM showing the impact on mean and diurnal harmonic of precipitation and compare these to observations.

The layout of this paper is as follows. In section 2 we briefly describe the physics parametrizations used in the Met Office climate model. Section 3 describes how the results of Stirling and Stratton (2011) can be used to change the mass flux scheme over land. Section 4 shows how the modified entrainment rates alter SCM UM simulations of the idealized CRM cases. Results from testing the changes in a full atmospheric model in climate mode are described in section 5, and a summary is given in section 6.

2. Description of the Unified Model physical parametrizations

This study uses both SCM and climate model versions of the UM (Cullen, 1993) to test changes to the convective parametrization scheme. Details of the main model physical

parametrizations are outlined below, with the model convective parametrization described in more depth. Not all parametrizations are used in the SCM configuration and the differences are outlined in section 4.1.

2.1. Radiation

The configuration of the UM that is used here uses the Edwards–Slingo radiation scheme (Edwards and Slingo, 1996) and the following aerosols (Bellouin *et al.*, 2007) are included: sulphate aerosols, black carbon, mineral dust (Woodward, 2001) and biogenic aerosols. In the climate model simulations the radiation scheme is called every 3 hours.

2.2. Boundary layer

A non-local mixing scheme is used for unstable boundary layers (Lock *et al.*, 2000) and a local Richardson number scheme for stable layers (Smith, 1990, 1993).

2.3. Large-scale clouds and micro-physics

The cloud scheme is the new prognostic cloud scheme known as PC2 (Wilson *et al.*, 2008a, 2008b). The micro-physics is a mixed-phase scheme including prognostic ice and liquid water (Wilson and Ballard, 1999).

2.4. Land surface scheme

The model's land surface scheme (MOSES-II; Essery *et al.*, 2001) is used with nine surface types. A coastal tiling scheme is used around the edges of land masses to ensure the atmospheric model matches the ocean model when run in coupled mode.

2.5. Gravity wave drag

The gravity wave drag parametrization is described in Webster *et al.* (2003) and includes flow blocking.

2.6. Convection

The convection scheme currently used in the Met Office UM is a mass flux scheme based on Gregory and Rowntree (1990) with various extensions to include downdraughts (Gregory and Allen, 1991) and convective momentum transport (CMT) (Gregory *et al.*, 1997; Stratton *et al.*, 2009). Further extensions include a separate diagnosis of deep and shallow convection starting from the boundary layer, with mid-level convection operating above. The current convection scheme, like most convective parametrization, is designed to model equilibrium convection. Diurnal convection over land is a form of non-equilibrium convection, i.e. the forcing is changing rapidly over the course of the day.

2.6.1. Diagnosis

The convective diagnosis is used to determine whether convection is possible from the boundary layer and, if so, whether the convection is deep or shallow. The convective diagnosis is based on an undilute parcel ascent from the near surface. This forms part of the boundary layer scheme

identifying unstable boundary layers (Lock *et al.*, 2000). Shallow convection is diagnosed if one of the following sets of conditions is met:

- The parcel attains neutral buoyancy below 2.5 km and there is descending air above.
- The parcel attains neutral buoyancy below the freezing level if this is higher than 2.5 km and there is descending air above.
- There is a strong inversion below 2.5 km with descending air above.
- There is a strong inversion below the freezing level with descending air above.

The descending air condition was found to be necessary as otherwise too much shallow convection was diagnosed. Strictly speaking, the diagnosis of shallow convection in the model includes some convection, which is often termed congestus. All other convection initiated from the boundary layer top is diagnosed as deep convection. Neither the shallow convection scheme nor the deep convection scheme is designed to explicitly model congestus convection.

2.6.2. Bulk cloud model used in the shallow, deep and mid-level schemes

From Gregory and Rowntree (1990) the equation for the bulk mass flux of the convection is given by

$$\frac{\partial M_p}{\partial p} = (E - N - D), \quad (1)$$

where

- M_p is the cloud mass flux of an ensemble of convective plumes
- p is the pressure
- $E = \epsilon M_p$ is the entrainment rate of the ensemble
- $N = \eta M_p$ is the mixing detrainment rate
- $D = \delta M_p$ is the forced detrainment rate
- ϵ, η, δ are fractional entrainment/detrainment rates.

The entrainment rate represents the amount of environmental air mixed with cloud air in the ensemble of convective plumes. The detrainment rates represent the amount of cloud air mixed back into the environment at any level. The bulk cloud model holds the mean properties of the ensemble of plumes at any model level.

2.6.3. Deep convection

The deep scheme still uses the original Gregory and Rowntree (1990) entrainment rate (in units of Pa^{-1}):

$$\epsilon = 3A_E \frac{p}{p_*}, \quad (2)$$

where p_* is the surface pressure and A_E is 1.5 for all levels above the lifting condensation level (LCL). The deep mixing detrainment rate depends on relative humidity (RH):

$$\eta = f(1 - \text{RH})\epsilon, \quad (3)$$

where $f = 1.0$. The forced detrainment rate has also been altered to be adaptive to the buoyancy of convection (Derbyshire *et al.* (2011)).

The deep convection scheme uses a convective available potential energy (CAPE) closure based on Fritsch and Chappell (1980). In the full model, to help suppress grid point storms, we use a CAPE closure that is modified by vertical velocity so that the CAPE time-scale is reduced if the vertical velocity in a column exceeds a threshold value. The CAPE time-scale used in our simulations is 2 hours. The convective momentum transport has also been changed to use a flux gradient approach (Stratton *et al.*, 2009).

2.6.4. Shallow convection

The shallow convection scheme can produce precipitation and uses a closure based on Grant (2001), with separate entrainment and detrainment rates consistent with observations and large eddy simulations.

The shallow entrainment rates at a given pressure p are given by

$$\epsilon = 0.03 \frac{w_*}{m_b} \frac{1}{\Delta p_{\text{cld}}} \exp\left(\frac{p - p_{\text{cldbase}}}{\Delta p_{\text{cld}}}\right), \quad (4)$$

where ϵ has units of Pa^{-1} , and w_* is the sub-cloud velocity scale in m s^{-1} ; m_b is the cloud base mass flux in units of m s^{-1} ; and Δp_{cld} is the pressure difference across the convective cloud estimated from the undilute diagnosis. The shallow entrainment rates tend to be larger than the deep entrainment rates. The shallow detrainment rate, D , is taken to be

$$\eta = 1.3\epsilon, \quad (5)$$

if RH is ≤ 0.85 and

$$\eta = \left(1 + 0.3 \left[\frac{1 - \text{RH}}{0.15}\right]\right)\epsilon, \quad (6)$$

for RH > 0.85 . The shallow detrainment rates are also greater than the values used in the deep scheme.

The shallow convective momentum transport uses flux–gradient relationships (Grant and Brown, 1999) derived from CRM simulations of shallow convection.

2.6.5. Mid-level convection

The mid-level convection scheme operates on any instabilities found in a column above the top of the deep/shallow convection or at least one model level above the LCL. The mid-level scheme closely resembles the original Gregory–Rowntree mass flux scheme with the original extensions (original CMT) but uses a CAPE closure. The entrainment and detrainment rates are similar to the deep scheme. In our current model mid-level convection tends to operate overnight over tropical land. It is not usually active in the development stage of the diurnal cycle.

3. Changes to the convection scheme

This section describes the changes made to the convective parametrization scheme in this study to improve the diurnal

cycle. These alterations apply only to points classed as land (i.e. points with a land fraction > 0.8 for coastal locations). The changes apply to those points diagnosed as deep by the convective diagnosis.

3.1. Deep entrainment rates

The key findings from the CRM study in Stirling and Stratton (2011) that we use here are as follows:

1. The shape of the CRM ensemble mean entrainment rate with height has an approximate n/z dependence.
2. The entrainment and detrainment rates in the early stages of convection are dependent on cloud size, with smaller clouds having larger entrainment/detrainment rates than those used at present (see Eqs (2) and (3)). The original idea of the entrainment rate depending inversely on cloud radius in cumulus models comes from Simpson and Wiggert (1969) and Simpson (1971).
3. The CRM simulations from Stirling and Stratton (2011) show that, over land, cloud area can initially be linked to the boundary layer depth or LCL, which can be evaluated from the model. The idea of linking entrainment rate to boundary layer depth is not new. It is used as a modification to the Arakawa–Schubert parametrization (Arakawa and Schubert, 1974), by Tokioka *et al.* (1988), to provide a minimum entrainment rate for a spectral convection scheme.

For simplicity, we choose to ignore the sensitivity to stability and relative humidity found in the CRM study, and concentrate on isolating the impact of cloud area on convective development. While there are a number of ways this can be represented, we choose to use the following formulation for n in the n/z entrainment rate (units m^{-1}):

$$n = 0.55 + 8.0 \left(1.2 - \frac{z_{\text{cl}}}{1000} \right)^2, \quad (7)$$

with upper and lower bounds of

$$0.55 \leq n \leq 3.5$$

which is found to give good agreement with the CRM results (see Figure 2 in section 4, where described).

For land points we alter the entrainment rates used by deep convection so that they have an n/z dependence, where z is the height above the surface and n has the dependence given by Eq. (7). Figure 1 compares the existing deep entrainment rates (calculated using a typical tropical pressure profile) and the range of entrainment rates used in the new scheme for land points. At low levels (< 5 km) the $1/z$ and $3.5/z$ entrainment rates (units m^{-1}) are much higher than the original deep convective entrainment rates.

3.2. Detrainment rates

Our changes to entrainment rates over land also alter our detrainment rates through the proportionality of Eq. (3). We have chosen to alter the detrainment rate for deep convection over land, making it more dependent on relative

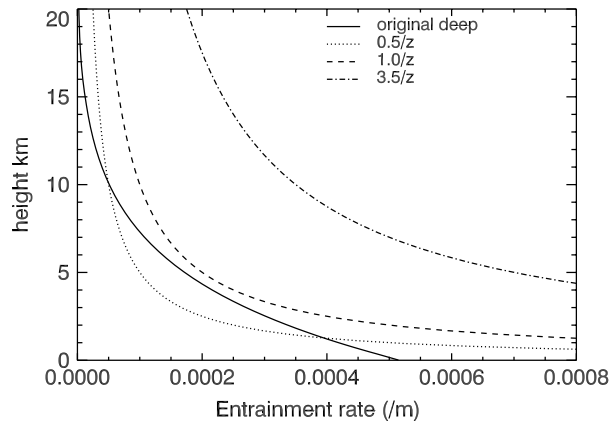


Figure 1. Plot of the convective deep entrainment rates currently used in the UM together with $0.55/z$, $1/z$ and $3.5/z$ entrainment rates.

humidity by increasing the factor f to 2.5 in Eq. (3). This decision was based on comparing the relative humidity of the CRM and SCM simulations (see section 4.5.2). SCM simulations that used a value of $f = 1$ tended to dry out the lower part of the troposphere where convection occurred. Increasing f to 2.5 tends to increase the mixing detrainment when the environment is drier and helps to raise the relative humidity.

3.3. Convective diagnosis

The diagnosis over land has been altered to perform both a dilute parcel ascent using the entrainment rates from section 3.1 and the original undilute ascent. The convection type is deduced as follows. If the dilute ascent finds convection is not possible (i.e. the parcel is no longer buoyant) but the undilute ascent suggests that convection is possible, no convection from the boundary layer is diagnosed, i.e. neither the shallow nor the deep convection schemes are called. If both the undilute and the dilute parcel ascents diagnose shallow convection then the shallow scheme is called and the entrainment rates used are as Eq. (4). If, however, the dilute ascent diagnoses shallow but the undilute diagnoses deep, the deep scheme is called and the new entrainment rates from Eq. (7) are used.

Over the sea, while the scheme itself has not been changed, the diagnosis uses a dilute parcel ascent with an entrainment rate of $0.55/z$ in units of m^{-1} . This may result in slightly more shallow convection being diagnosed over the ocean.

4. Idealized SCM simulations of the diurnal cycle

4.1. SCM model

In this section we show how application of the new deep entrainment rates alters the representation of deepening convection in a single-column model. We explore its performance for a range of environmental conditions in which both relative humidity and atmospheric stability are altered (see Table I; Stirling and Stratton, 2011). The SCM simulations are designed to be directly comparable to the CRM study in Stirling and Stratton (2011), and results from the SCM and CRM studies are compared. A set of control SCM simulations were run to see how well the SCM with no changes is able to simulate the diurnal cycle. This control set will be known as SCM1. A second set of SCM simulations

were run with the changes to the convection scheme described in section 3 and this will be known as SCM2.

The SCM in this study is based on the Met UM configuration described in section 2, with 70 levels in the vertical as used in the Met Office's global operational numerical weather prediction model from 2009. The simulations use a 10-minute time step for both convection and the rest of the physics. We choose to set the SCM to a sea point to avoid the complications of initializing soil moisture, soil temperature and deciding on appropriate vegetation cover, but the convection scheme treats it as a land point. The diurnal cycle over land is simulated by forcing the SCM with strongly varying surface sensible and latent heat fluxes more appropriate to a land surface. In the diurnal SCM runs described here the model radiation scheme is switched off, to remove additional forcing arising from convective cloud feedback. Removing cloud forcing in the SCM simulations allows us to see whether we can improve the height of convective cloud tops without having to get their cloud forcing correct. Achieving a good convective cloud forcing in the UM is no longer dependent solely on the convection scheme but is strongly influenced by the coupling between the convection scheme and PC2, the prognostic cloud scheme.

4.2. SCM forcing

The surface latent and sensible heat fluxes are specified every 30 minutes, the values being taken from the CRM runs where the fluxes increase sinusoidally, reaching a peak of 553 W m^{-2} in the latent heat and 270 W m^{-2} in the sensible heat. These values are interpolated linearly in time to match the SCM model time step. The hourly mean radiative forcing from the CRM is used to force the SCM. The surface conditions for the SCM are set up to be the same as the CRM.

4.3. Results from SCM runs and comparison with CRM

Figure 2 shows the development of convection from 7.30 am to 10 am local solar time for the complete set of runs. The CRM simulations show a gradual development of convection growing in height over this period. Where the profiles are more unstable (right-hand column) and the RH higher (top row), the convection develops to greater height more rapidly. Although these simulations are for a tropical environment they are consistent with the RH and stability dependence found in the mid-latitude ARM observational study of Zhang and Klein (2010). The lifting condensation level (cloud base) increases slowly with time.

4.3.1. SCM1: control simulations

In the case of the control set of SCM simulations, deep convection is diagnosed from the first time step. The deep scheme immediately operates up to the height achieved by the CRM towards the end of the period, and tends to be intermittent (i.e. on then off on alternate time steps), particularly for the more unstable cases. The SCM1 simulated cloud tops tend to fall towards the end of the period, e.g. R95, R75, R74, so that the depth of the convection becomes lower than the CRM. Overall, the original convection scheme does a poor job of simulating the development phase of the diurnal cycle of convection

over land but it does achieve about the correct height for the fully developed deep convection.

4.3.2. SCM2: changes to improve diurnal cycle

The SCM simulations were rerun making the changes described in section 3 to the convection scheme over land. Figure 2 also shows the results from the SCM2 simulations. The use of a dilute parcel ascent (using high entrainment rates as the LCL is low) in the diagnosis routine delays the first diagnosis of convection by a few time steps, the delay being longer for the lower RH cases. No shallow convection was diagnosed in the SCM2 as was the case in SCM1. Use of increased entrainment rates (i.e. rates dependent on the height of LCL) in the deep scheme results in convection terminating at lower levels, particularly in the lower relative humidity cases. In the high RH cases (first row, Figure 2), deep convection is suppressed for a few time steps but when diagnosed rapidly attains a height of at least 7 km and then grows very slowly afterwards, failing to reach the final CRM height. The initial rate of growth of deep convection is still too quick for the high RH cases, though it is significantly improved for the lower (10–50%), more stable cases. When deep convection is diagnosed, e.g. R55, there is an initial period of shallower deep convection, a jump in convective cloud top and then a gradual continued growth similar to the CRM simulation. Another improvement seen in all the SCM2 simulations is more continuous convection. Only in the most unstable and higher humidity cases do the SCM2 simulations start to show intermittent deep convection towards the end of the period. The CAPE closure used in the deep convection scheme uses the CAPE evaluated over the depth of the deep convection. In the earlier stages of the convection where the depth of convection is lower, the diagnosed CAPE will be lower, so the convective increments applied will be smaller. This accounts for the smoother deep convection in the early stages of the simulations. When larger convective increments are applied they can result in the lower layers being stabilized, preventing convection on the next time step. Overall, the SCM2 simulations of convective cloud top give much better agreement with the CRM results.

Various questions can be asked about our changes to the deep convection scheme:

- How does switching to an n/z entrainment rate compare with the original height dependence given by Eq. (2)? Running the SCM with a fixed $0.55/z$ entrainment rate gives very similar results to SCM1.
- Could we have improved the diurnal cycle over land by just increasing entrainment rates like Wang *et al.* (2007); i.e. is the link to a time-dependent entrainment rate really needed? The answer to this is that tests increasing entrainment rate by a fixed amount, e.g. to use $3.5/z$, will delay convection in our model by the order of an hour but will also tend to lower the maximum height attained by the deep convection by several kilometres. Similarly, if we used the entrainment rate in Eq. (2) but increased by a factor of 1.5, we would delay deep convection but we would also lower the maximum height. Therefore increasing entrainment rate alone is not enough; the time dependence is required.
- What difference does the increase in detrainment factor, f , have? Increasing the detrainment factor leads

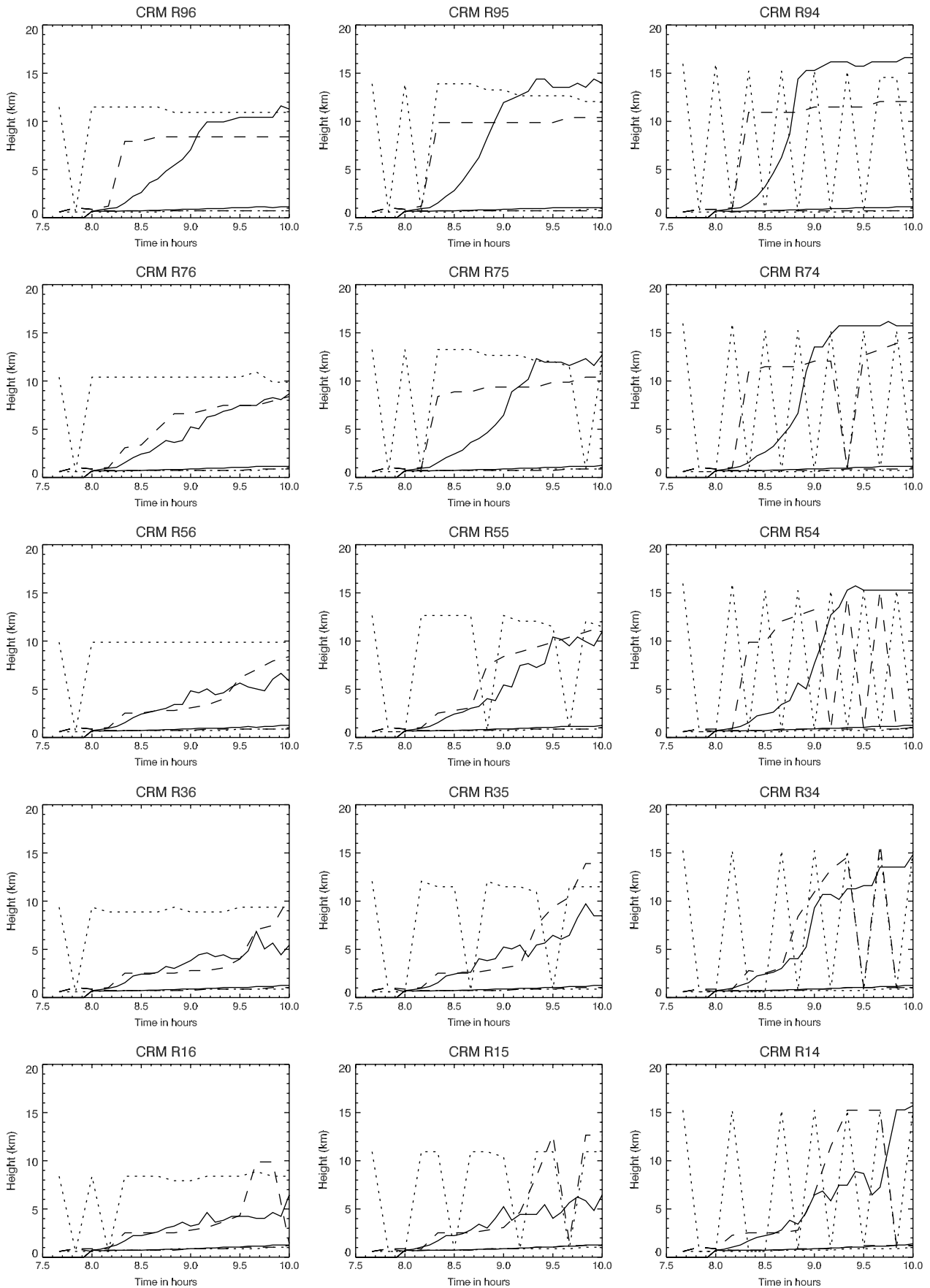


Figure 2. Time series of cloud base and top from the CRM results (solid line), SCM1 (dotted line) and SCM2 (dashed line) for the 15 diurnal cases. CRM runs are labelled, e.g. R96, where the 9 indicates the initial (in this case) 90% relative humidity and the 6 the model stability. The lower the number, the less stable.

to an earlier transition to deeper convection for RH of 30–50%. It tends to moisten the mid troposphere in better agreement with the CRM simulations. It has no impact on higher RH.

- The CRM study implies an n/z dependence where $n \propto 1/z_{cl}$; here in Eq. (7) we have used a stronger dependence on the lifting condensation level as we found it gave slightly better results when used in the SCM. The important feature of the expression for n is that it varies from a high entrainment of order 3.5 to a low entrainment of order 0.55 over a range of lifting condensation heights.

5. Full atmosphere-only climate tests

The SCM tests show that it is possible in the case of idealized diurnal cycle simulations to have a significant impact on the convective behaviour. The real test of any change to the convection scheme is how it behaves in a full global model. We choose to test the changes in an atmosphere-only version of the climate model. The version used is close to GA1.0, a development version of HadGEM3-A, run at N96L38 resolution (i.e. 1.875×1.25 latitude with 38 model levels). The climate model simulations are forced using AMIP II (Gates *et al.*, 1999) sea surface temperatures and sea ice starting from September 1978. Two ten-year simulations were run:

- Control—no changes to the convection scheme.
- New run—the changes to the diagnosis and convection over land as described in section 3.

The aim of the two runs is to see whether the changes have a beneficial impact on the diurnal cycle. To assess the diurnal cycle of convection over land we follow the approach taken by others (e.g. Lin *et al.*, 2000; Yang and Slingo, 2001) and look at the diurnal harmonics of precipitation.

5.1. Precipitation observations

To assess the diurnal cycle of precipitation over land we require a widespread climatology of precipitation with information on the diurnal variation of precipitation. TRMM (the Tropical Rainfall Measurement Mission satellite; Simpson *et al.*, 1988) provides a source of detailed precipitation measurements at high spatial and time resolution. We use the TRMM 3B42 products available from NASA to form a climatology of 3-hourly observations of precipitation for the region 50°N – 50°S during the period 1998–2006. The raw $0.25^\circ \times 0.25^\circ$ data have been re-gridded to the climate model grid (i.e. 1.875° longitude \times 1.25° latitude). While we have used the TRMM 3B42 products as these were readily available, a comparison study (Dai *et al.*, 2007) of various precipitation climatologies containing diurnal information suggests that satellite products like TRMM 3B42 (i.e. from infrared data) may tend to give a time of maximum precipitation over land which is the order of 1–2 hours later than surface observations. Climatologies from TRMM microwave data have an earlier peak, in better agreement with surface observations. A more recent study (Hirose *et al.*, 2008) compares TRMM precipitation radar data (a more definitive method of measuring precipitation)

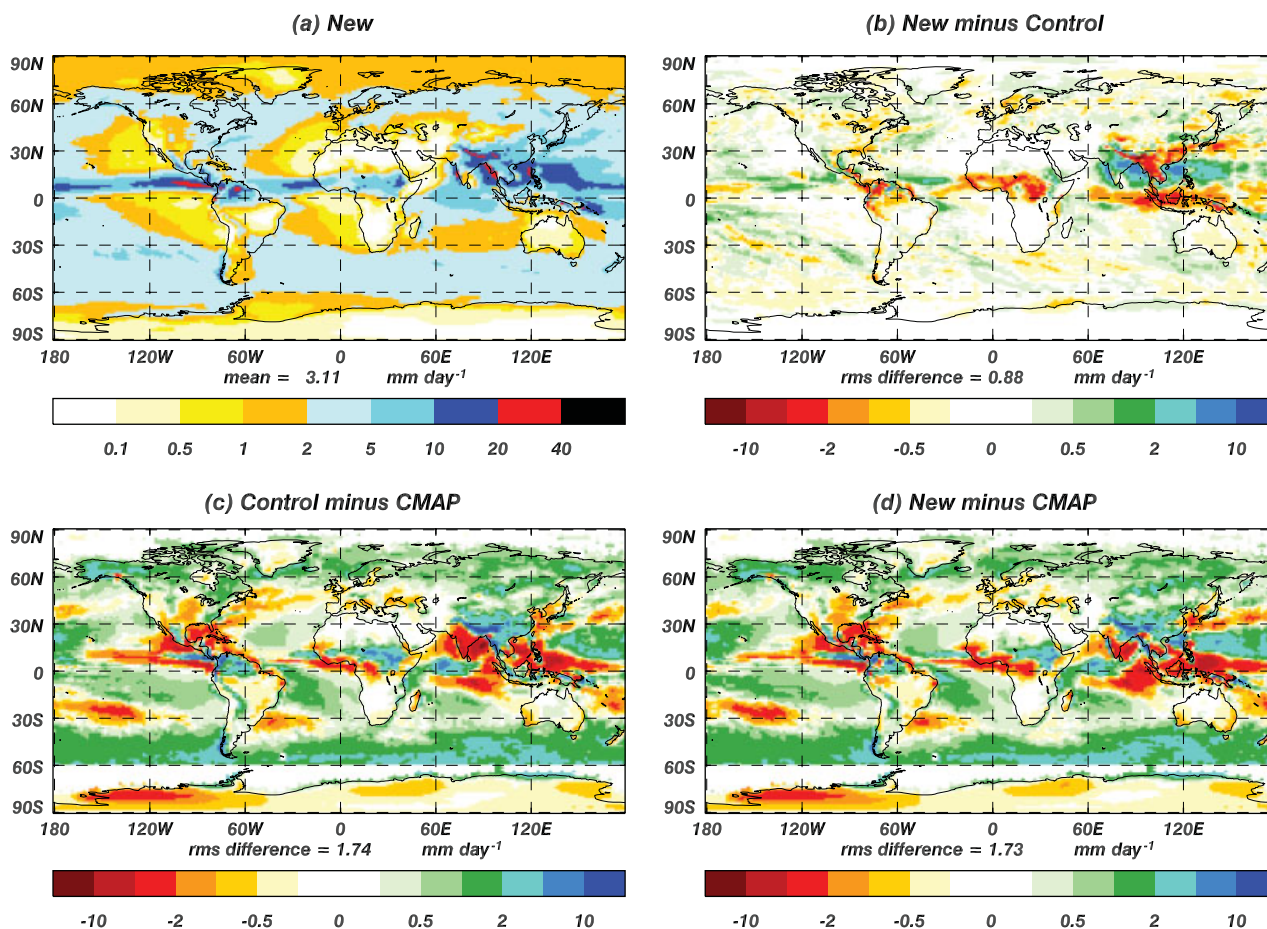


Figure 3. Mean precipitation for JJA (a) new run, (b) new run minus control, (c) control minus CMAP, (d) new run minus CMAP.

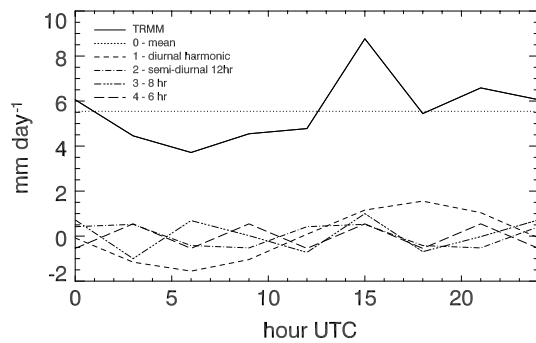


Figure 4. Mean diurnal cycle of TRMM precipitation for JJA for a grid point at 10°N, 0°E, with a breakdown into its Fourier components.

with TRMM microwave data and finds differences in the timing of the peak in precipitation, but uses a different method of defining the peak so cannot be readily compared with this study. Given errors of the order of 6–7 hours in the phase of the control run (see section 5.3.2) we considered it to be within acceptable margins to use the TRMM 3B42 observations as the basis for our study.

5.2. Analysis of the climate model mean precipitation

Before assessing the diurnal component of the precipitation it is important to know how well the climate model is able to simulate the mean precipitation. Figure 3 shows the model control and new runs compared against the global CMAP (Climate Prediction Centre Merged Analysis of Precipitation) climatology of precipitation (Xie and Arkin, 1997) for JJA (June July August). The global mean bias for JJA when compared with CMAP is unchanged at 0.34 mm per day. The control integration (Figure 3(c)) tends to lack

precipitation over India and have too much precipitation over tropical land in Africa and in South America. The new run has generally reduced the precipitation over tropical land, tending to improve agreement with CMAP. The increase in precipitation over India is beneficial, though the Indian monsoon flow is now strong, extending out into the western Pacific. In DJF (December January February) (not shown), there is a similar reduction over tropical land, generally improving agreement with CMAP. The diurnal change has not improved the lack of precipitation over the maritime continent in any season.

At mid latitudes the changes in precipitation are smaller. Western Europe is slightly drier in JJA, making agreement with CMAP worse, but further east over Europe a slight increase tends to improve agreement with CMAP.

5.3. Analysis of the diurnal cycle of precipitation

Three-hourly mean precipitation was averaged over the different seasons to give the mean 3-hourly precipitation for each 3-hour period of the day. The eight 3-hourly means were then analysed using Fourier analysis to calculate the diurnal harmonic, i.e. the amplitude and phase of the fit to a single sine wave in 24 hours. Figure 4 illustrates the Fourier decomposition for a location over tropical Africa. The peak in the TRMM data is at 1500 UTC but the peak in the diurnal harmonic is later. In this paper, when we refer to the phase of the peak in precipitation we are referring to the phase of the peak in the diurnal harmonic.

5.3.1. Amplitude of the diurnal harmonic of precipitation

In all seasons the amplitude of the diurnal cycle harmonic of precipitation is reduced, giving better agreement with

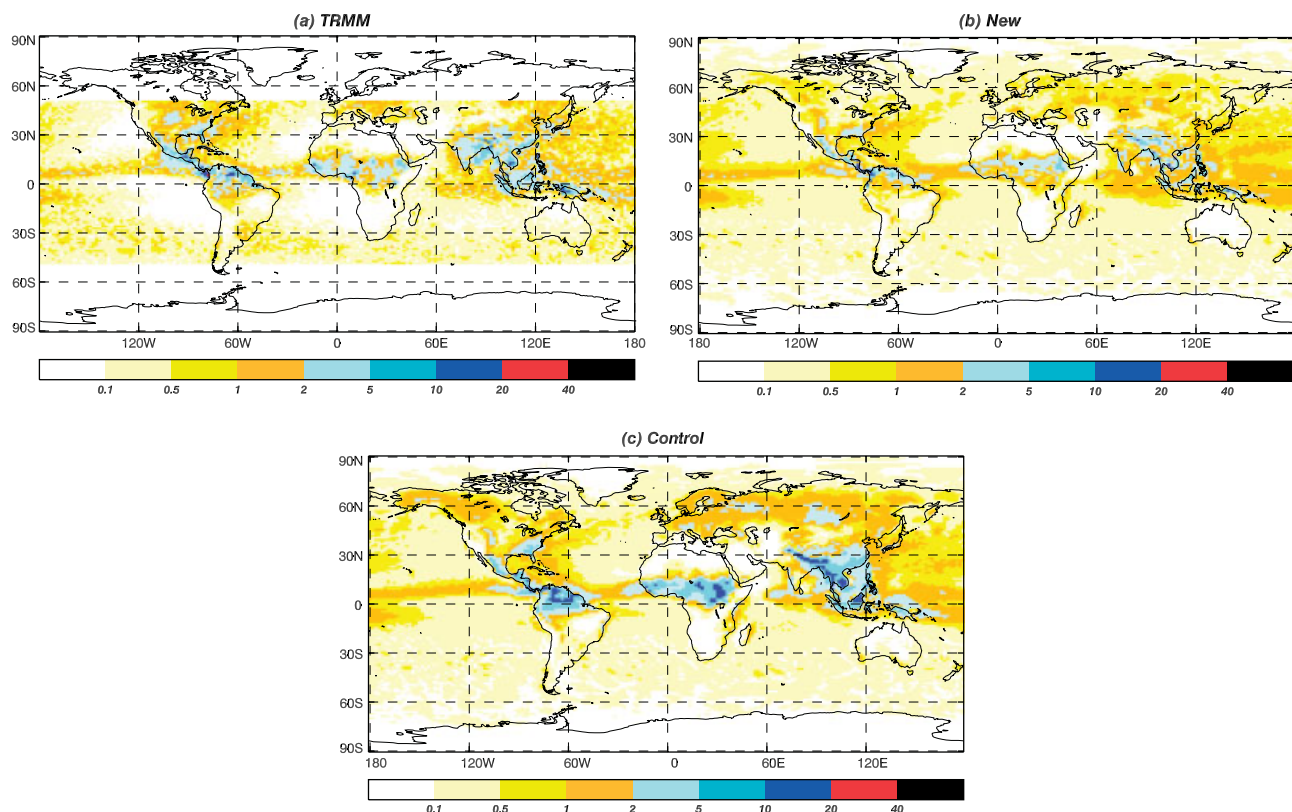


Figure 5. Amplitude of the diurnal harmonic of precipitation for (a) TRMM, (b) new run, (c) control run. Units: mm per day.

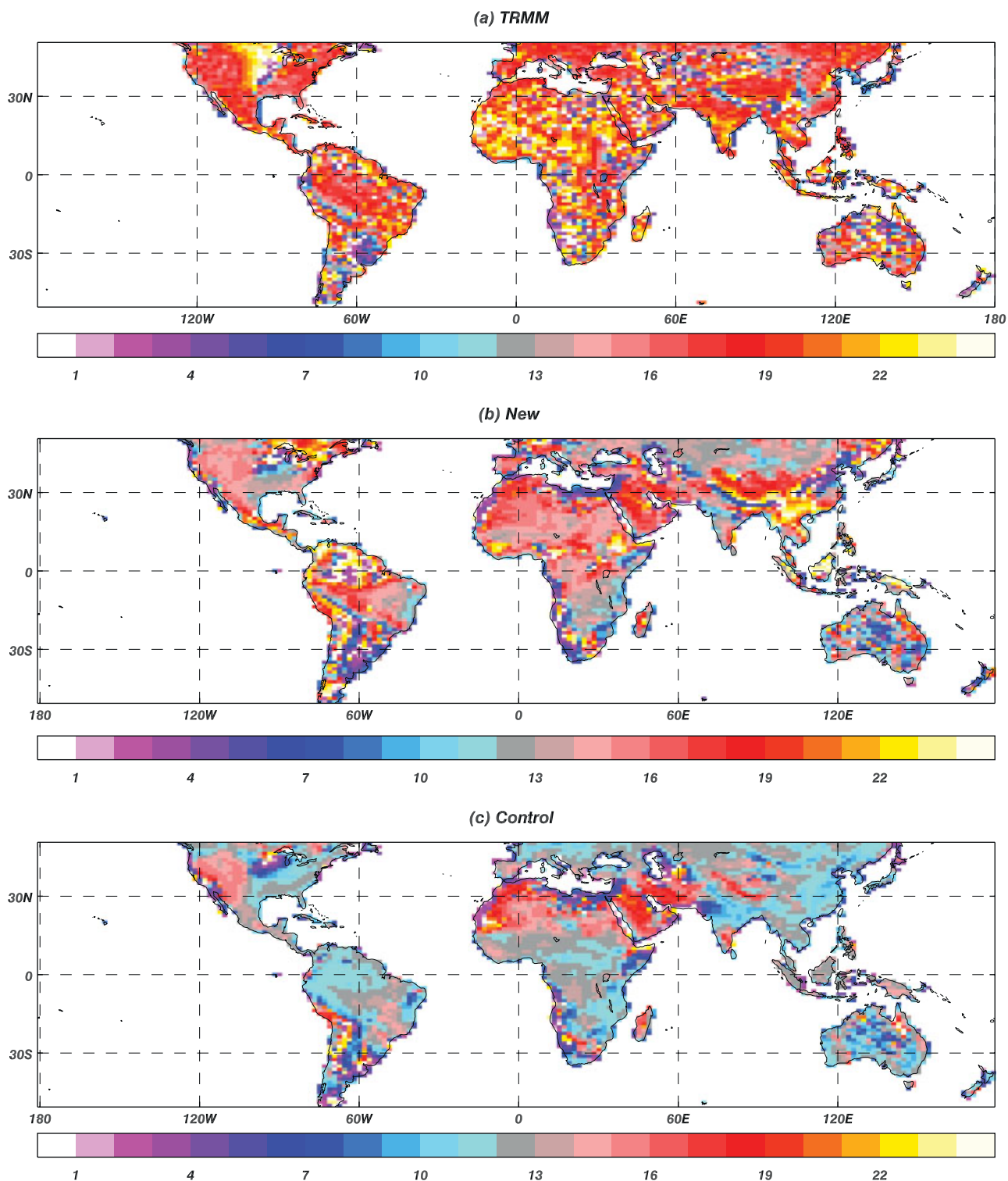


Figure 6. The local time of maximum of the diurnal harmonic of precipitation for JJA (a) TRMM data, (b) new run, (c) control run.

TRMM observations. For land points between 50°N and 50°S the overall mean amplitude of the diurnal harmonic for the four seasons for TRMM is 1.13 mm per day; for the control 2.06 mm per day and for the new run 0.88 mm per day. In both simulations the amplitude of the diurnal cycle is largest over the land (see Figure 5) for JJA. In the control run the amplitude tends to be too high over tropical land, much of equatorial Africa being above 5 mm per day, whereas TRMM has 2–5 mm per day. The new run has a lower amplitude over land (2–5 mm per day) tending now to be a little too low in some areas. Over the

maritime continent, where the mean precipitation has been reduced below observed values, the amplitude of the diurnal harmonic is now too low. At mid latitudes over Europe, Russia and North America the amplitude of the diurnal cycle is now a smaller proportion of the mean precipitation. Dai *et al.* (2007) suggest that the ratio of the amplitude of the diurnal harmonic to the mean precipitation for JJA over mid-latitude land should be between 20% and 50%, depending on the satellite data used. In the control run the value is of the order 50–70%, with reduced values in the range 10–40% in the new run.

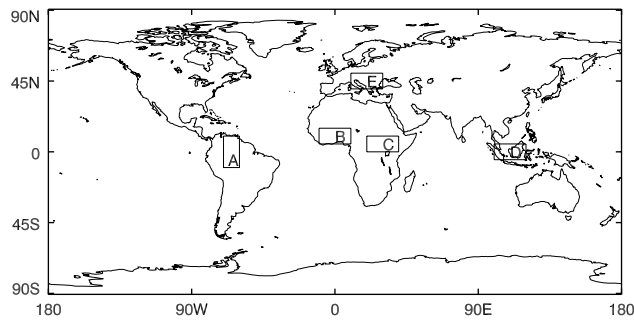


Figure 7. Map showing the location of the five areas: A, South America, 10°N–10°S, 60–70°W; B, West Africa, 5–15°N, 10°W–10°E; C, East Africa, 0–10°N, 20–40°E; D, maritime continent, 5°N–5°S, 100–120°E; E, Europe, 40–50°N, 10–30°E.

No significant changes in the diurnal cycle of precipitation over the oceans are found. This is expected as the only change to the convective parametrization on ocean points is the change to using a dilute parcel ascent (with an entrainment rate of $0.55/z \text{ m}^{-1}$), which may result in a slightly higher frequency of diagnosis of shallow convection. There is a reduction in the amplitude over the sea surrounding the maritime continent (Figure 5), making agreement with TRMM worse. While the agreement over the oceans is good, the amplitude of the diurnal harmonic is too large over the Subtropics to the west of the continents. This may be explained by the high mean precipitation in these regions (Figure 3). The diurnal amplitude for DJF (not shown) shows very similar changes to JJA, i.e. a smaller amplitude in the diurnal run, agreeing better with TRMM.

5.3.2. Phase of the diurnal cycle

The phase of the peak in the diurnal harmonic over land can vary widely over the globe (see Figure 6(a)), depending on location, but an overall value gives an initial indication of the performance of the changes. To do this the phase of the peak in diurnal harmonic was analysed for all four seasons over land points between 50°N and 50°S. The mean time for the phase from the TRMM data was found to be 15.6 hours, while identical analysis for the control gives 12.2 hours and for the new run 14.5 hours. The change is therefore giving an improvement in the mean value of the order of 2 hours.

Figure 6 shows how the phase of the diurnal cycle of precipitation varies over the globe. Over most land the maximum in observed precipitation occurs in the late afternoon and into the evening (Figure 6(a)). In contrast, the control run shows the precipitation occurring as early as 9–10 am local solar time in the morning over parts of tropical South America. In the new simulation we have delayed the peak in the precipitation over most tropical land by several hours, improving agreement with TRMM observations. Over tropical South America the peak is now about 1–2 hours too late, whereas over equatorial Africa the peak is still 1–2 hours early.

Figure 8 shows the JJA diurnal cycle of total precipitation for five regions of the globe (see Figure 7) broken into contributions from the different schemes. For all five regions the amplitude of the total precipitation has been reduced, making it closer to the TRMM data except in the case of area E (Europe). The very large peak in the control precipitation is replaced by a lower peak occurring later in the day in many cases, i.e. areas A, C, D and E. Looking

at the convective contributions to the total precipitation, Figure 8 (central column) shows that in all areas the deep contribution has been reduced and in the cases of areas C and E slightly delayed. The mid-level component has increased in the evening for all areas. This suggests that the suppression of deep convection during the day is leaving a more unstable profile in the evening, resulting in more mid-level convection overnight. Most areas show very little change to the large-scale component of precipitation (Figure 8, right-hand column).

In area B (western Africa), more shallow convection is diagnosed, suggesting the circulation has altered. Looking at a plot of the occurrence of shallow convection for this region in JJA (not shown) suggests we are increasing the shallow convection in the south of the region near the coast but not further to the north.

In area D the suppression of deep convection has resulted in the new run having a later peak than TRMM. The maritime continent (area D), however, is a very difficult region to model at the resolution used in this study because convection over the islands is controlled predominantly by land sea breezes which are not resolved in the model.

The European region (area E) has weaker diurnal forcing, with some days being convectively forced and others not in JJA. Deep convection has been damped earlier in the day but does not persist later into the evening.

5.4. Analysis of other changes

5.4.1. General circulation

Overall, the introduction of the entrainment changes does not have a large impact on the general circulation of the climate model as is illustrated by the Taylor diagram (Taylor, 2001; Figure 9(a)). This is calculated by comparing the ten-year multi-annual seasonal means on their latitude–longitude grids from the control and new runs for a wide selection of model fields. The radius of the Taylor diagram plots the mean standard deviation of the grid points for each seasonal mean about the mean value of the field normalized by the mean standard deviation of the climatological seasonal means also computed on the same latitude longitude grid. The angle from the vertical plots the spatial correlation coefficient between the grid points of the model and the climatology for the four seasonal means. The normalized root mean square error of the model field compared with the climatology is given by the distance from the point marked 'Obs' to the plotted location.

Table I gives a description of the fields and the climatologies used for the comparison. The new run shows an improvement on the control if the symbol plotted on the diagram is closer to the point marked 'Obs'. In both DJF and JJA there is a slight strengthening of the Hadley circulation which is already too strong (see changes in the 850 and 200 hPa V component of winds, Figure 9(a)). The (~ 1 K) warm bias in the upper-tropical troposphere is very slightly reduced in the zonal mean for both DJF and JJA, illustrated by the improvement in the 200 hPa temperature in Figure 9(a). There is no noticeable difference in the zonal mean relative humidity of the model. This is not unexpected as we are only delaying deep convection during the early part of the day over land and not suppressing it completely. At tropical latitudes there is more sea than land so the

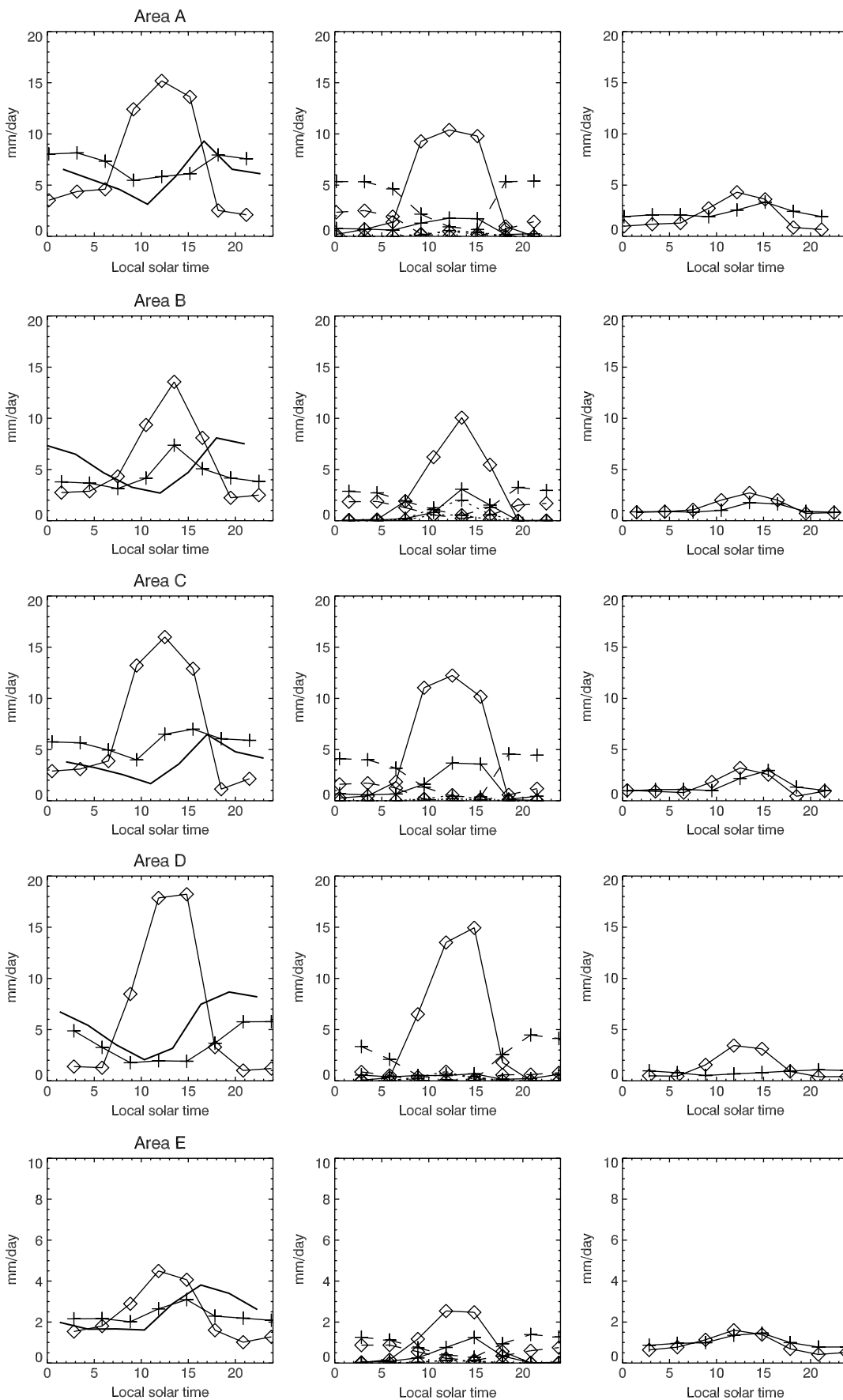


Figure 8. Mean JJA diurnal cycle of precipitation for the five regions given in Figure 7. Left-hand column shows total precipitation, TRMM as a solid line, control as a line with squares and new as a line with plus symbols. The central column shows the breakdown of the convective precipitation for the control (square) and new (plus) into deep convective (solid line), shallow convective (dotted line) and mid level (dashed line). The right-hand column shows the large-scale component of the precipitation with control (square) and new (plus).

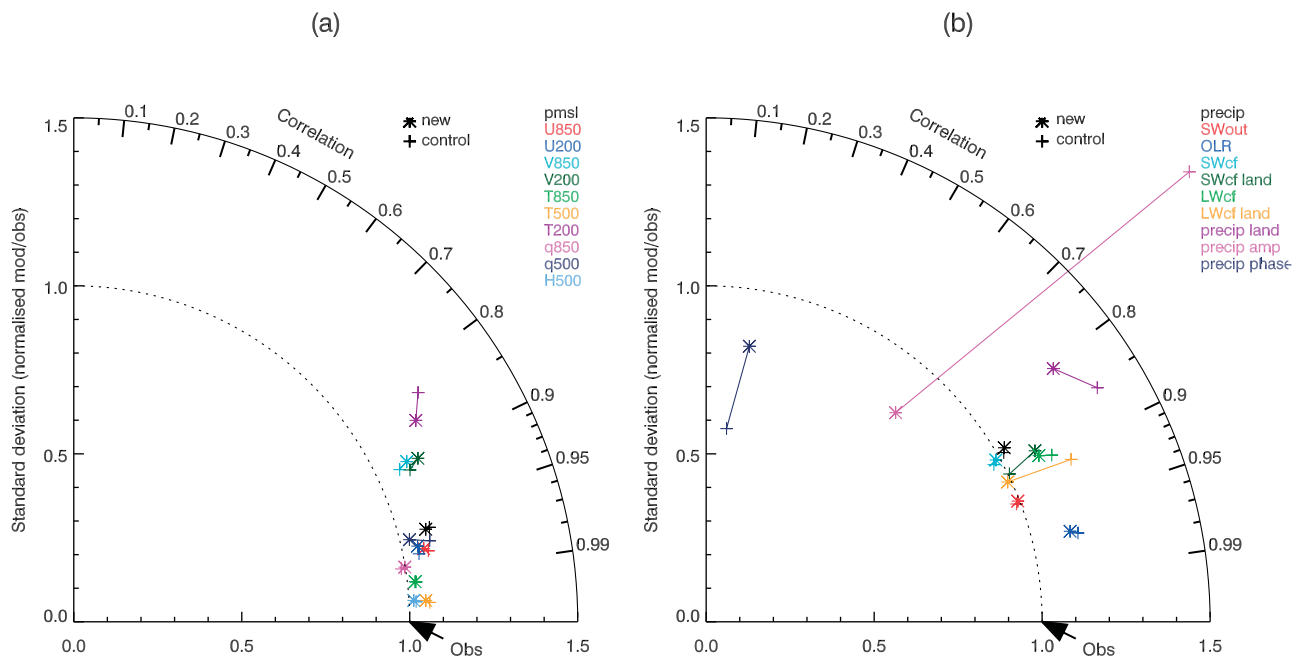


Figure 9. Taylor diagrams comparing ten-year multi-annual season means with various climatologies: (a) various fields on pressure levels; (b) precipitation and radiation fields. See Table I for key to fields.

Table I. Climatologies used for comparison with the model simulations.

Field (units)	Climatology used
PMSL—mean sea-level pressure (Pa)	ERA—interim
U 850 hPa—U component of wind ($m s^{-1}$)	ERA—interim
U 200 hPa—U component of wind ($m s^{-1}$)	ERA—interim
V 850 hPa—V component of wind ($m s^{-1}$)	ERA—interim
V 200 hPa—V component of wind ($m s^{-1}$)	ERA—interim
T 850 hPa—temperature (K)	ERA—interim
T 500 hPa—temperature (K)	ERA—interim
T 200 hPa—temperature (K)	ERA—interim
q 850 hPa—specific humidity ($kg kg^{-1}$)	ERA—interim
q 500 hPa—specific humidity ($kg kg^{-1}$)	ERA—interim
H 500 hPa—height (m)	ERA—interim
precip—total precipitation (mm per day)	CMAP
Swout—TOA outgoing short wave ($W m^{-2}$)	CERES
OLR—TOA outgoing long wave ($W m^{-2}$)	CERES
SWCF—short-wave cloud forcing ($W m^{-2}$)	CERES
SWCF land—over land $50^{\circ}N-50^{\circ}S$	CERES
LWCF—long-wave cloud forcing ($W m^{-2}$)	CERES
LWCF land over land $50^{\circ}N-50^{\circ}S$	CERES
precip land—precipitation over land $50^{\circ}N-50^{\circ}S$	TRMM
amp—amplitude of diurnal harmonic over land	TRMM
phase—phase of peak in diurnal harmonic (land)	TRMM

zonal mean is weighted to the behaviour over the sea. The main difference between the simulations occurs in JJA when the monsoon circulation is strengthened, as mentioned in section 5.2.

5.4.2. Changes to cloud and radiation

Altering the diurnal cycle of convection over land should alter the diurnal cycle of clouds over land and hence the diurnal cycle of radiation. The diurnal cycle of top-of-atmosphere outgoing long-wave radiation (OLR) was improved in the Hadley Centre climate model with the introduction of the PC2 cloud scheme (Wilson *et al.*, 2008b), which detrained cloud condensate directly from the deep convection scheme. The cloud condensate tended to remain overnight, representing anvils. In the new simulation, the mean OLR over tropical land is increased, tending to improve biases when compared with observations (CERES Clouds and the Earth’s Radiant Energy System; (Wielicki *et al.*, 1996) in DJF and JJA for most locations.

Figure 9(b) shows a selection of radiation fields on a Taylor diagram together with precipitation. The global mean errors in short-wave and long-wave radiation are not very different in the new run. Looking over land between $50^{\circ}N$ and $50^{\circ}S$ the long-wave cloud forcing shows an improvement, with the new run having a standard deviation the same as the observations. Conversely, for the short-wave cloud forcing over land there is a slight degradation, with the new run having higher variability with the correlation decreasing. The changes we have made to the entrainment and detrainment rates and to the occurrence of deep convection over land have resulted in less ice cloud being detrained; hence the OLR is increased relative to the control. More liquid water cloud has been detrained lower in the atmosphere in the early stages of convection, leading to a larger short-wave cloud forcing over some land regions.

The Taylor diagram (Figure 9(b)) also shows the same analysis for the diurnal harmonic of precipitation for the four seasons over land between $50^{\circ}N$ and $50^{\circ}S$. It is clear from this diagram that we have improved the standard deviation of the diurnal amplitude so that it is closer to the observations. The standard deviation of phase relative has

become closer to the observations and the level of spatial correlation has increased.

6. Summary

This paper shows that the use of a variable entrainment rate can improve the representation of the diurnal cycle in a climate model with little detriment to the mean fields.

- The key change to the convective parametrization over land was to make the entrainment rates decrease with increasing LCL, which was used as a proxy for cloud area early in the day.
- The SCM simulations of the development phase of convection over land show that the change to the parametrization is able to delay the development of deeper convection, in better agreement with CRM results.
- The changes to the convection scheme have made little change to the overall climate simulation. The only negative feature is a slight strengthening of the Hadley circulation, which was already too strong. The largest change is to the monsoon circulation in JJA, which has resulted in a beneficial increase of precipitation over India, but a detrimental increase in the strength of the 850 hPa wind flow.
- The mean precipitation and the amplitude of the diurnal harmonic over land are reduced over most regions, improving overall agreement with observations. Also, the time of the local maximum in precipitation is delayed, giving better agreement with TRMM 3B42 observations. It is possible that for a few locations our changes have resulted in the transition to deeper convection being suppressed too much, so that precipitation over land is now too low relative to observations.
- The changes to the convection and hence to precipitation and clouds over land do not have any large adverse impacts on the already fairly good diurnal cycle of OLR over land.

Although the amount of precipitation in the evening is increased in the new simulation, there may be scope to further improve the decay phase of the diurnal cycle, e.g. by using a wake parametrization (Rio *et al.*, 2009) to prolong the instability in the boundary layer. This will be investigated in future work, together with the processes controlling growth and decay of convection over the oceans. The eventual aim is to come up with a unified approach to entrainment over both land and sea.

Acknowledgements

The TRMM 3-hourly precipitation data came from the NASA Goddard Space Flight Center Data Archive. CERES data were obtained from the NASA Langley Research Center Atmospheric Sciences Data Center. We thank Dan Bernie, who obtained and processed the 3-hourly TRMM data, creating the multi-annual means we used in this study; Adrian Lock for advice on improving the model stability and useful discussions on our results; and Roy Kershaw, Andy Brown, Martin Willett and Gill Martin for useful comments on our paper. We thank our reviewers for their feedback, which has helped improve our paper.

References

- Arakawa A, Schubert WH. 1974. Interactions of a cumulus cloud ensemble with the large-scale environment. Part 1. *J. Atmos. Sci.* **31**: 674–701.
- Bechtold P, Chaboureaud J-P, Beljaars A, Betts AK, Kohler M, Miller M, Redelsperger J-L. 2004. The simulation of the diurnal cycle of convective precipitation over land in a global model. *Q. J. R. Meteorol. Soc.* **130**: 3119–3137.
- Bellouin N, Boucher O, Haywood J, Johnson C, Jones A, Rae J, Woodward S. 2007. *Improved representation of aerosols for HadGEM2*. Hadley Centre Technical Note 73. Met Office: Exeter, UK.
- Cullen MJP. 1993. The unified forecast/climate model. *Meteorol. Mag.* **122**: 81–94.
- Dai A, Lin X, Hsu KL. 2007. The frequency, intensity, and diurnal cycle of precipitation in surface and satellite observations over low- and mid-latitudes. *Clim. Dynam.* **29**: 727–744.
- Del Genio AD, Wu J. 2010. The role of entrainment in the diurnal cycle of continental convection. *J. Climate* **23**: 2722–2738.
- Derbyshire SH, Maidens AV, Milton SF, Stratton RA, Willett M. 2011. Adaptive detrainment in a convective parametrization. *Q. J. R. Meteorol. Soc.* **137**: 1856–1871.
- Edwards JM, Slingo A. 1996. Studies with a flexible new radiation code. I: Choosing a configuration for a large-scale model. *Q. J. R. Meteorol. Soc.* **122**: 689–720.
- Emanuel KA. 1991. A scheme for representing cumulus convection in large-scale models. *J. Atmos. Sci.* **48**: 2313–2335.
- Essery R, Best M, Cox P. 2001. *MOSES 2.2 technical documentation*. Hadley Centre Technical Note 30. Met Office: Exeter, UK.
- Fritsch J, Chappell C. 1980. Numerical prediction of convectively driven mesoscale pressure systems. Part I: Convective parameterization. *J. Atmos. Sci.* **37**: 1722–1733.
- Gates WL, Boyle JS, Covey C, Dease CG, Doutriaux CM, Drach RS, Fiorino M, Gleckler J, Hnilo JJ, Marlais SM, Phillips TJ, Potter GL, Santer BD, Sperber KR, Taylor KE, Williams DN. 1999. An overview of the results of the Atmospheric Model Intercomparison Project (AMIP I). *Bull. Am. Meteorol. Soc.* **80**: 29–55.
- Grabowski WW, Bechtold P, Cheng A, Forbes R, Halliwell C, Khairoutdinov M, Lang S, Nasuno T, Petch J, Tao W-K, Wong R, Wu X, Xu K-M. 2006. Daytime convective development over land: A model intercomparison based on LBA observations. *Q. J. R. Meteorol. Soc.* **132**: 317–344.
- Grant ALM. 2001. Cloud-base fluxes in the cumulus-capped boundary layer. *Q. J. R. Meteorol. Soc.* **127**: 407–421.
- Grant ALM, Brown AR. 1999. A similarity hypothesis for shallow-cumulus transports. *Q. J. R. Meteorol. Soc.* **125**: 1913–1936.
- Gregory D, Allen S. 1991. 'The effect of convective downdraughts upon NWP and climate simulations'. In *Ninth Conference on Numerical Weather Prediction*, Denver, CO; 122–123.
- Gregory D, Rowntree PR. 1990. A mass-flux convection scheme with representation of cloud ensemble characteristics and stability dependent closure. *Mon. Weather Rev.* **118**: 1483–1506.
- Gregory D, Kershaw R, Inness PM. 1997. Parametrization of momentum transport by convection. II: Tests in single column and general circulation models. *Q. J. R. Meteorol. Soc.* **123**: 1153–1183.
- Guichard F, Petch JC, Redelsperger J-L, Bechtold P, Chaboureaud J-P, Cheient S, Grabowski W, Grenier H, Jones CG, Kohler M, Piriou J-M, Tailleux R, Tomasimmi M. 2004. Modelling the diurnal cycle of deep precipitating convection over land with cloud-resolving models and single-column models. *Q. J. R. Meteorol. Soc.* **130**: 3139–3172.
- Hirose M, Oki R, Shimizu S, Kachi M, Higashiuwatoko T. 2008. Finescale diurnal rainfall statistics refined from eight years of TRMM PR data. *J. Appl. Meteorol. Clim.* **47**: 544–561.
- Khairoutdinov M, Randall D. 2006. High-resolution simulations of shallow-to-deep convection transition over land. *J. Atmos. Sci.* **63**: 3421–3436.
- Kuang Z, Bretherton CS. 2006. A mass-flux scheme view of a high-resolution simulation of a transition from shallow to deep cumulus convection. *J. Atmos. Sci.* **63**: 1895–1909.
- Lin X, Randall DA, Fowler LD. 2000. Diurnal variability of the hydrological cycle and radiative fluxes: comparisons between observations and a GCM. *J. Climate* **13**: 4159–4179.
- Lock AP, Brown AR, Bush MR, Martin GM, Smith RNB. 2000. A new boundary layer mixing scheme. Part I: Scheme description and single-column model tests. *Mon. Weather Rev.* **128**: 3187–3199.
- Rio C, Hourdin F, Grandpeix J-Y, Lafore J-P. 2009. Shifting the diurnal cycle of parametrized deep convection over land. *Geophys. Res. Lett.* **36**: L07809, DOI: 10.1029/2008GL036779.
- Simpson J. 1971. On cumulus entrainment and one-dimensional models. *J. Atmos. Sci.* **28**: 449–455.

- Simpson J, Wiggert V. 1969. Models of precipitating cumulus towers. *Mon. Weather Rev.* **97**: 471–489.
- Simpson J, Adler RF, North GR. 1988. Proposed tropical rainfall measuring mission (TRMM) satellite. *Bull. Am. Meteorol. Soc.* **69**: 278–295.
- Smith RNB. 1990. A scheme for predicting layer clouds and their water content in a general circulation model. *Q. J. R. Meteorol. Soc.* **116**: 435–460.
- Smith RNB. 1993. 'Experience and developments with the layer cloud and boundary layer mixing schemes in the UK Meteorological Office Unified Model'. In *ECMWF/GCSS Workshop on Parametrization of the Cloud-Topped Boundary Layer*. ECMWF: Reading, UK.
- Stirling A, Stratton RA. 2011. Entrainment processes in the diurnal cycle of deep convection over land. *Q. J. R. Meteorol. Soc.* DOI: 10.1002/qj.1868 (in press).
- Stratton RA, Stirling AJ, Derbyshire S. 2009. *Changes and developments to convective momentum transport (CMT) parametrization based on analysis of CRM and SCM*. Met R&D Technical Note 530. Met Office: Exeter, UK. <http://www.metoffice.gov.uk/publications>
- Taylor KE. 2001. Summarizing multiple aspects of model performance in a single diagram. *J. Geophys. Res.* **106**: 7183–7192.
- Tiedtke M. 1989. A comprehensive mass flux scheme for cumulus parametrization in large-scale models. *Mon. Weather Rev.* **117**: 1779–1800.
- Tokioka T, Yamazaki K, Kitoh A, Ose T. 1988. The equatorial 30–60 day oscillation and the Arakawa–Schubert penetrative cumulus parameterization. *J. Meteorol. Soc. Japan* **66**: 883–901.
- Wang Y, Zhou L, Hamilton K. 2007. Effect of convective entrainment/detrainment on the simulation of the tropical precipitation diurnal cycle. *Mon. Weather Rev.* **135**: 567–585.
- Webster S, Brown AR, Cameron DR, Jones CP. 2003. Improvements to the representation of orography in the Met Office Unified Model. *Q. J. R. Meteorol. Soc.* **129**: 1989–2010.
- Wielicki BA, Barkstrom BR, Harrison EF, Lee RB III, Smith GL, Cooper JE. 1996. Clouds and the Earth's Radiant Energy System (CERES): an Earth observing system experiment. *Bull. Am. Meteorol. Soc.* **77**: 853–868.
- Wilson DR, Ballard SP. 1999. A microphysically based precipitation scheme for the UK Meteorological Office Unified Model. *Q. J. R. Meteorol. Soc.* **125**: 1607–1636.
- Wilson DR, Bushell AC, Kerr-Munslow AM, Price JD, Morcrette CJ. 2008a. PC2: a prognostic cloud fraction and condensation scheme. I: Scheme description. *Q. J. R. Meteorol. Soc.* **134**: 2093–2107.
- Wilson DR, Bushell AC, Kerr-Munslow AM, Price JD, Morcrette CJ, Bodas-Salcedo A. 2008b. PC2: a prognostic cloud fraction and condensation scheme. II: Climate model simulations. *Q. J. R. Meteorol. Soc.* **134**: 2109–2125.
- Woodward S. 2001. Modelling the atmospheric life cycle and radiative impact of mineral dust in the Hadley Centre climate model. *J. Geophys. Res.* **106**: 18155–18166.
- Xie P, Arkin PA. 1997. Global precipitation: a 17-year monthly analysis based on gauge observations, satellite estimates, and numerical model outputs. *Bull. Am. Meteorol. Soc.* **78**: 2539–2558.
- Yang G-Y, Slingo JM. 2001. The diurnal cycle in the Tropics. *Mon. Weather Rev.* **129**: 784–801.
- Yang S, Smith EA. 2006. Mechanisms for diurnal variability of global tropical rainfall observed from TRMM. *J. Climate* **19**: 5190–5226.
- Zhang Y, Klein SA. 2010. Mechanisms affecting the transition from shallow to deep convection over land: inferences from observations of the diurnal cycle collected at the ARM Southern Great Plains Site. *J. Atmos. Sci.* **67**: 2943–2959.